Crystal structure of the Eg5 - K858 complex and implications for structure-based design of thiadiazole-containing inhibitors

Sandeep K. Talapatra[a,1], Chuin Lean Tham[a,1], Paolo Guglielmi[b], Roberto Cirilli[c], Balakumar Chandrasekaran[d], Rajshekhar Karpoormath[d], Simone Carradori[e] and Frank Kozielski[a]*

[a]School of Pharmacy, University College London, 29-39 Brunswick Square, London, WC1N 1AX, United Kingdom,

[b]Department of Drug Chemistry and Technologies, Sapienza University of Rome, P.le A. Moro 5, 00185 Rome, Italy,

[c]National Institute of Health, Centre for the Control and Evaluation of Medicines, Viale Regina Elena 299, 00161 Rome, Italy.

[d]Discipline of Pharmaceutcial Sciences, College of Health Sciences, University of KwaZulu-Natal (UKZN), Westville, Durban, 4001, South Africa,

[e]Department of Pharmacy, G. D'Annunzio University of Chieti/Pescara, Via dei Vestini 31, 66100 Chieti, Italy,

Corresponding author: f.kozielski@ucl.ac.uk

[1]Both authors contributed equally

Highlights

- Eg5 is a potential target for drug development in cancer chemotherapy
- The thiadiazole scaffold containing inhibitors target the Eg5 motor domain
- (S)-ARRY-520 has advanced to clinical phase III trials against multiple myeloma
- The Eg5-K858 complex provides crucial insights into this important chemical scaffold
- Using the crystal structure of the complex we rationalised our structure-activity relationship study

Keywords

1,3,4-thiadiazole, K858 enantiomers, Eg5, antimitotic drugs, Eg5-K858 complex, rational drug design

Abbreviations

KSP, Kinesin spindle protein; MT, Microtubule; PDB, Protein Data Bank; PK, Pyruvate kinase; LDH, Lactate dehydrogenase; ITC, Isothermal titration calorimetry; PIPES, Piperazine-*N*,*N′*-bis(2-ethanesulfonic acid); βMe, β-Mercaptoethanol; DMSO, Dimethylsulfoxide; rpm, rounds per minute; HEPES, 4-(2-Hydroxyethyl)-1-piperazineethanesulfonic acid; PEG, Polyethyleneglycol; MES, 2-(*N*-morpholino)ethanesulfonic acid; AU, Asymmetric unit; SAR, Structure-activity relationship.

Abstract

The thiadiazole scaffold is an important core moiety in a variety of clinical drug candidates targeting a range of diseases. For example, the 2,4,5-substituted 1,3,4-thiadiazole scaffold is present in a lead compound and at least two clinical candidates targeting the human motor protein Eg5, against neoplastic diseases. An inhibitor named K858 has *in vivo* activity in various mouse xenografts whereas the clinical candidates (S)-ARRY-520 and (R)-Litronesib have entered clinical trials with

the former one in phase III clinical trials either alone or in combination with a proteasome inhibitor against relapsed/refractory multiple myeloma. Astonishingly, structural data are lacking for all thiadiazole-containing Eg5 inhibitors. Here we report the structure determination of two crystal forms of the ternary Eg5-ADP-K858 complex, locking the motor in the so-called final inhibitor bound state, thus blocking ADP release, a crucial stage for Eg5 activity. K858 acts at the established allosteric inhibitor-binding pocket formed of helix α2, loop L5 and helix α3. The structure of the complex has far reaching consequences for thiadiazole containing Eg5 inhibitors. For example, we could rationalise the structure-activity relationship in the crucial 5-position of the thiadiazole scaffold and the complex will serve in the future as a basis for strucutre-based drug design.

1. Introduction

Established tubulin-targeting chemotherapeutic drugs such as taxanes and vinca alkaloids are clinically proven anti-cancer agents. They target the mitotic spindle, a molecular machinery made of microtubules (MTs), which is responsible for chromosome segregation during cell division [1-3]. However, MTs are also key components in neuronal transport, and their disruption can lead to serious toxic side effects such as neurotoxicity [4]. Therefore, certain mitotic kinesins are investigated for their potential as novel drug targets with the hope to develop complementary treatment options and to reduce side effects.

The mitotic kinesin Eg5 (also called Kif11, Kinesin Spindle Protein, KSP), a member of the kinesin-5 subfamily [5], is essential for establishing the bipolar mitotic spindle [6]. Structurally, Eg5 exists as a homotetramer via oligomerisation of the central stalk domain [7, 8]. As there is a second MT-binding site in the C-terminal tail domain, the quaternary structure of homotetrameric Eg5 imparts the functionality of crosslinking and sliding anti-parallel MTs apart, which is essential for centrosome separation during early stages of cell division [9].

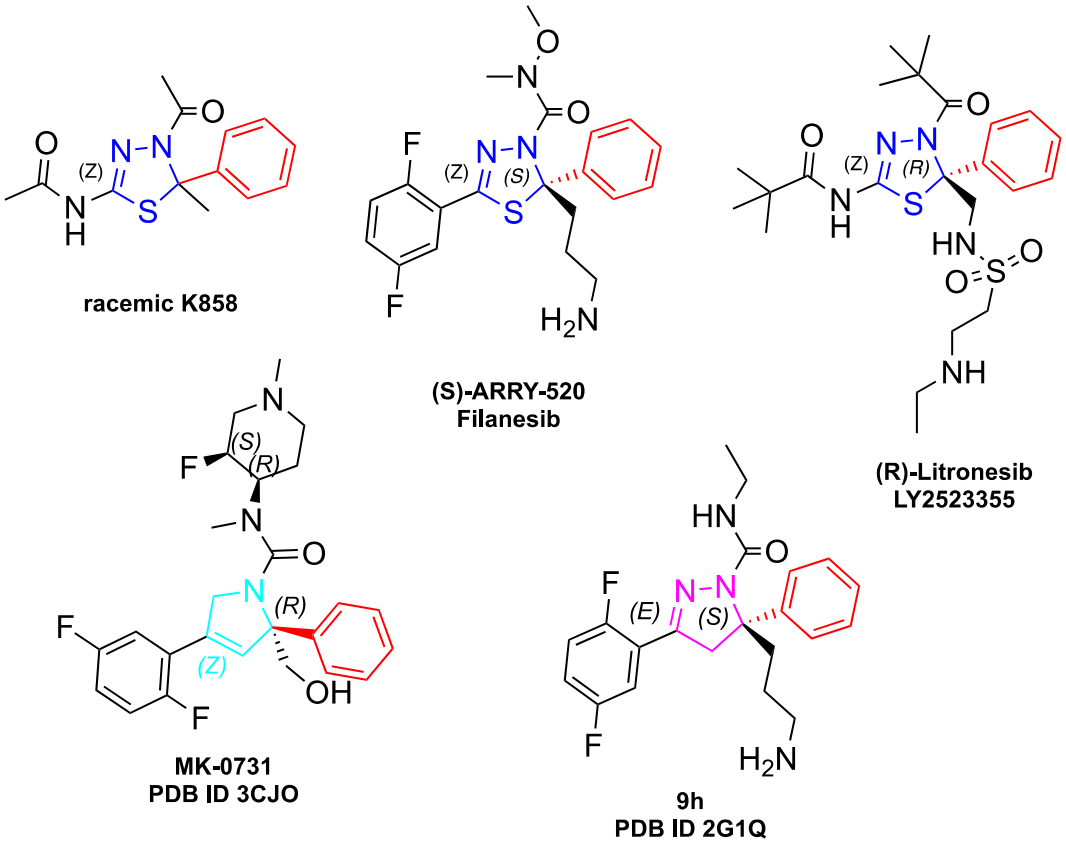

Figure 1: Chemical structures of related Eg5 inhibitors. Racemic K858, (S)-ARRY-520 (also known as Filanesib) and (R)-Litronesib (LY2523355) contain the 1,3,4-thiadiazole scaffold, which is coloured in blue. MK-0731 is a dihydropyrrole containing Eg5 inhibitor developed by Merck whereas compound **9h** contains a dihydropyrazole scaffold. Please also note that the 5-phenyl group is present in the chemical structures shown here and all inhibitors display a very similar 2,4,5 substitution pattern, sometimes even sharing identical substituents.

Eg5 has become an attractive target for drug development in cancer chemotherapy since the discovery of monastrol, the first selective inhibitor of Eg5 [10]. The inhibition of Eg5 results in the formation of monopolar spindles, which leads to mitotic arrest and may lead to subsequent apoptotic cell death. As Eg5 is crucial and specific for mitosis, its inhibition would achieve anti-mitotic effects with fewer and less undesirable effects than have been observed for tubulin targeting agents [11-14]. Today, several inhibitors targeting Eg5 have entered phase I, II and III clinical trials either as monotherapies or in combination with other drugs [15].

Clinical candidates targeting Eg5 show a variety of chemically distinct scaffolds, with thiadiazole-based (S)-ARRY-520 (Figure 1) being the most encouraging inhibitor to enter phase III clinical trials as a combination therapy with a proteasome inhibitor for the treatment of multiple myeloma [16, 17]. Despite of the promising clinical results, it remains to be established where exactly (S)-ARRY-520 binds to the motor domain of Eg5 to exert its highly specific inhibitory effects. The structural information is urgently needed to understand why (S)-ARRY-520 is so successful in advancing into phase III clinical trials.

Another clinically relevant Eg5-targeting inhibitor containing the thiadiazole scaffold is (R)-Litronesib (also named LY2523355). (R)-Litronesib (Figure 1) causes mitotic arrest and apoptotic cell death in tumour cells and has been shown to be active in a variety of mouse xenograft tumour models [18]. Dose finding and dose-escalating studies were conducted in a range of phase I clinical trials in advanced solid tumours [19, 20] in preparation for phase II trials. Later, it was shown that (R)-Litronesib displayed chiral instability leading to racemisation of the active enantiomer [21]. Eventually, the drug candidate was discontinued for strategic reasons [22].

K858, the third example of an Eg5 inhibitor containing the thiadiazole as a core scaffold and which is structurally related to (S)-ARRY-520 and (R)-Litronesib (Figure 1), was first discovered in a phenotype-based screen as a novel Eg5-specific inhibitor [23]. Racemic K858 (rK858) inhibited the MT-stimulated Eg5 ATPase activity (IC_{50} = 1.3 µM) in an ATP-uncompetitive manner. It induced monoastral spindles, mitotic arrest and subsequent cells death in HTC116 tumour cells. It did not inhibit other human kinesins tested and did not influence MT dynamics *in vitro* nor had a detectable effect on the MT network in cells, indicating specificity for Eg5. Even though it was not a very potent inhibitor against the MT-stimulated ATPase activity, it inhibited tumour growth in an A2780 ovarian cancer xenograft model and did not exhibit any neurotoxicity in this animal model. Importantly, it was also able to induce cell death in paclitaxel-resistant cancer cells, suggesting that rK858 may serve as a starting point for the development of more potent anti-cancer agents, based on the thiadiazole scaffold.

Recently, it has been shown that rK858 induces apoptosis and reverses the malignant invasive phenotype in human glioblastoma cells [24] and also influences

survivin-related chemoresistance in breast cancer cells [25]. While the anti-Eg5 and anti-tumour activities of rK858 have been characterised in cell-based assays and *in vivo*, the biochemical and structural basis for inhibiting Eg5 not only by rK858, but also for the other two thiadiazole containing derivatives (S)-ARRY-520 and (R)-Litronesib, are still unknown. Here, we further describe the inhibition effects of rK858 using biochemical and biophysical assays. We also determined two distinct crystal structures of the ternary complex of the human Eg5 motor domain in complex with Mg^{2+}ADP and K858. Our crystal structures reveal important structural insights into how thiadiazole-containing compound binds to the allosteric drug-binding pocket of Eg5. This provides a first glimpse of the important thiadiazole scaffold as a potent inhibitor of Eg5 and has implications for further structure-based design. Finally, we conducted a structure-activity relationship (SAR) study by determining the IC_{50} values for 46 analogues of K858 and rationally interpreted the results using the structure of the complex as a basis.

2. Results and Discussion

For biochemical experiments and co-crystallisation, rK858 was synthesised as previously described [26, 27] and its synthetic route is presented in **Scheme 1** as a representative example for the thiadiazole derivatives (**1-46**) measured in this study. Acetophenone (**a**) in methanol was reacted with thiosemicarbazide (**b**) under vigorous stirring to afford (*E*)-2-(1-phenylethylidene)hydrazine-1-carbothioamide (**c**) quantitatively. The ^{1}H NMR data of **c** revealed that a singlet peak resonating at δ 10.27 ppm was attributed to the –NH proton. One of the thioamidic protons (-C=(S)NH_2) appeared as a singlet at δ 8.26 ppm, while the other proton had merged with the aromatic protons in the aromatic region between δ 7.91 - 7.93 ppm. Moreover, the methyl (CH_3) protons resonated at δ 2.29 ppm. In ^{13}C NMR, we observed a characteristic peak at δ 178.93 ppm which indicated the presence of the C=S functionality. The compound **c** undergoes a cyclisation and a subsequent acetylation reaction in acetic anhydride to give *N*-(4-acetyl-5-methyl-5-phenyl-4,5-dihydro-1,3,4-thiadiazol-2-yl)acetamide (**1**) as a racemic mixture. The formation of **1** was confirmed by the presence of two additional methyl group protons appearing as

distinctive singlets at δ 2.01 ppm and δ 2.19 ppm in the shielded region of ^{1}H NMR. This has been further established in ^{13}C NMR where two new methyl group (CH_3) carbons appeared at δ 23.6 ppm and δ 26.5 ppm. In addition, two new carbonyl carbons (C=O) were also recorded at δ 167 and 169 ppm, respectively. Thus the structure of compound **1** (rK858), was confirmed based on ^{1}H and ^{13}C NMR spectral data, which corroborated with previous literature [23]. The syntheses and characterisation of the 46 selected K858 analogues investigated in our SAR study were recently described [28].

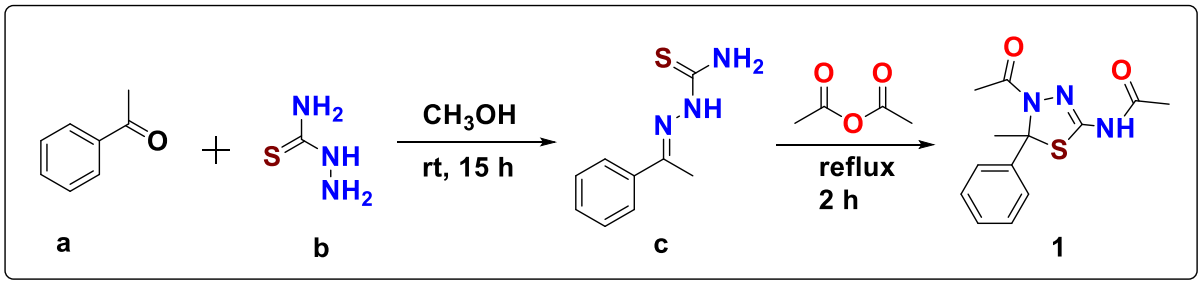

Scheme 1: Synthetic route for rK858 [26, 27].

2.1 Biochemical and biophysical characterisation of inhibition of Eg5 by rK858

Although the inhibitory effect of rK858 on the MT-stimulated Eg5 ATPase activity has been reported [23], we were curious whether rK858 was also able to directly bind to and inhibit the basal ATPase activity of Eg5. rK858 was capable of inhibiting the basal ATPase activity of Eg5 with an IC_{50} value of 740 ± 0.4 nM (Figure 2A). To verify the inhibition of the MT-stimulated ATPase activity, the assays were repeated in the presence of MTs and we obtained an IC_{50} value of 738 ± 0.3 nM, similar to the value obtained by Nakai and close to the IC_{50} value for the inhibition of the basal ATPase activity (Figure 2B) [23, 29]. As a complementary assay, we also employed isothermal titration calorimetry (ITC) to determine the binding affinity of rK858 for Eg5. ITC analysis revealed that rK858 is a nanomolar inhibitor that tightly binds to Eg5 with a K_d value of 664.5 ± 0.7 nM, with one inhibitor molecule bound per catalytic domain of Eg5 (Figures 2C).

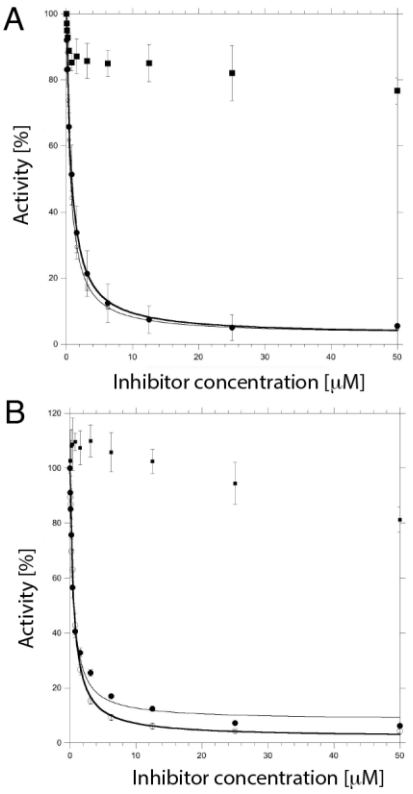

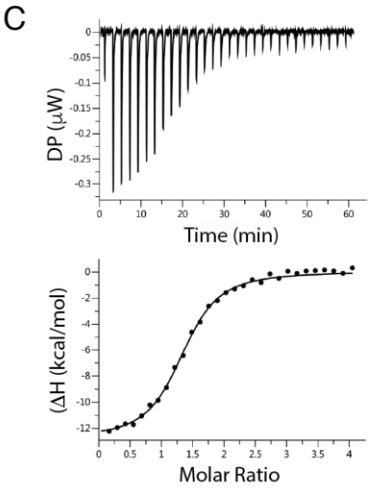

D

Inhibitor	*n*	K_d(nM)	ΔH	ΔTS	ΔG
rK858	1.2 ± 0.14	664.5 ± 0.71	-13.0 ± 0.14	-8.4 ± 0.01	-4.5 ± 0.13
K858-1	0.8 ± 0.06	220.0 ± 4.21	-24.1 ± 0.35	-9.1 ± 0.01	-15 ± 0.42
K858-2	no inhibition				

Figure 2: Biochemical and biophysical characterisation of the Eg5-K858 complex. A) Concentration-response plots of K858 for the inhibition of the basal Eg5 ATPase activity. Inhibition of the basal ATPase activity by rK858 (●), the first eluted K858 enantiomer on the Chiralpak IA column (K858-1) (■), and the second eluted enantiomer K858-2 (□). B) Concentration-response plots of K858 for the inhibition of the MT-stimulated Eg5 ATPase activity. Inhibition of the MT-stimulated ATPase activity by rK858 (●), the first eluted K858 enantiomer (K858-1) (■), and the second eluted enantiomer K858-2 (□). C) ITC analysis of the Eg5-K858 interaction. The raw ITC data of the binding reaction between Eg5 and rK858 is shown in the upper panel. The lower panel shows normalised ITC data plotted against the molar ratio of inhibitor to protein. The data fits very well to the single-site binding model. D) Thermodynamic parameters, K_d of binding and stoichiometry for rK858 and the two enantiomers K858-1 and K858-2 obtained from the ITC experiments.

2.2 Overall structure of the ADP-Eg5-K858 ternary complex

Since rK858 was capable to bind to and inhibit the basal ATPase activity of Eg5, this allowed us to set up crystallisation trials of the Eg5-K858 complex, in order to determine the structure of the ADP-Eg5-K858 ternary complex. We were able to crystallise the Eg5-rK858 complex in two distinct space groups and to determine the structures for both complexes, albeit at distinct resolutions (Table 1). In space group $C222_1$, crystals diffracted to 1.8 Å resolution and contained one Eg5-rK858 complex per asymmetric unit (AU). In contrast, in the second condition, crystals formed in space group $P6_522$ with one molecule in the AU, but diffracted to only 2.8 Å resolution. In both crystal forms the complex structures represent the final inhibitor bound state. In this conformation, the switch II cluster is in the permissive position, allowing the neck-linker to dock to the motor domain (Figure 3A and B). In the two molecules of the two distinct crystal forms, rK858 binds to the same pocket in an identical orientation. Due to the significantly higher resolution of the first crystal form, we will concentrate our subsequent structure interpretation using the high-resolution complex present in the $C222_1$ complex.

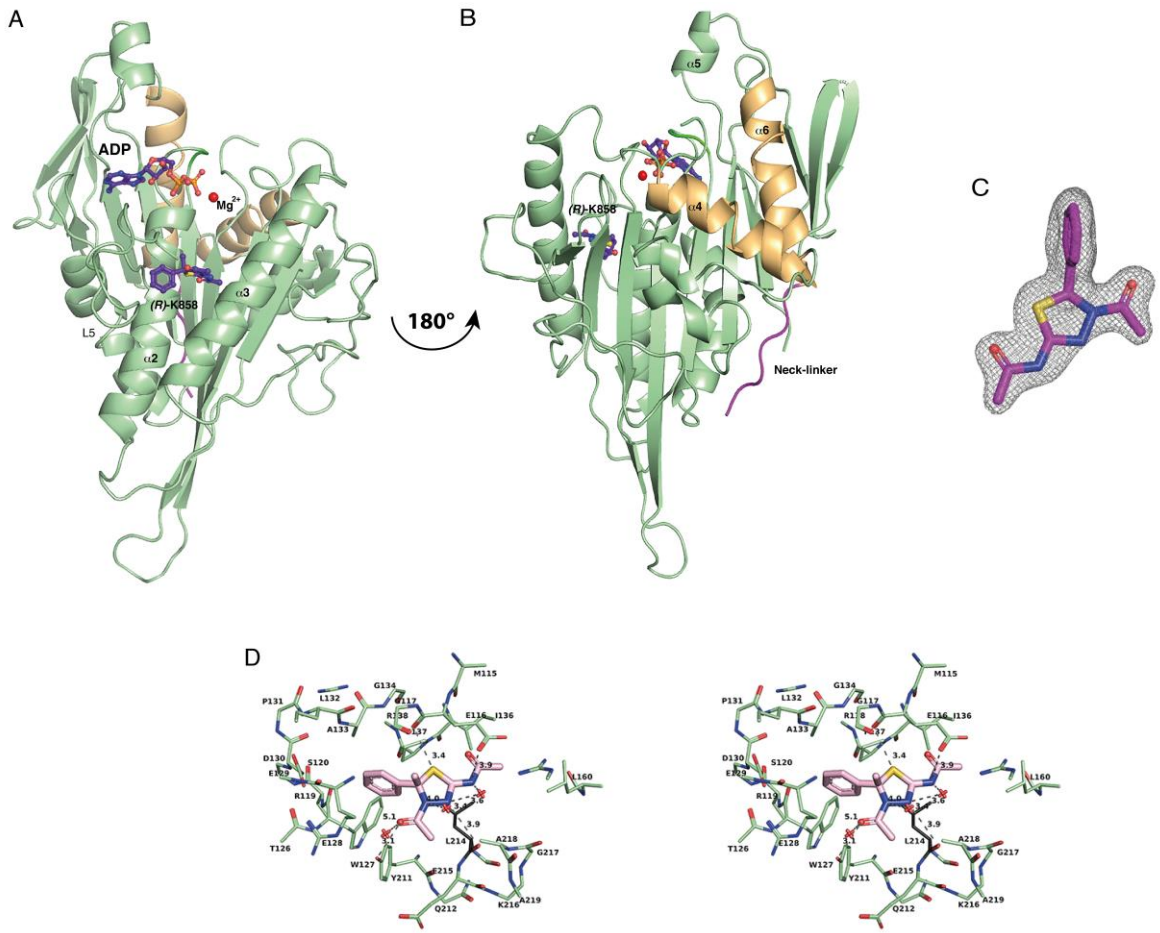

Figure 3: Overall structure of the Eg5-ADP-(R)-K858 complex. A) Front view of the overall structure of the Eg5 motor domain with bound Mg^{2+}ADP in the nucleotide-binding pocket. (R)-K858 (magenta) is located in the allosteric helix α2/loop L5/helix α3 inhibitor-binding pocket. Both, Mg^{2+}ADP and (R)-K858 are shown as ball-and-stick models. B) Back view showing that the switch II region is in the so-called permissive orientation (coloured in orange) allowing the neck linker (shaded in purple) to dock to the motor domain. C) (R)-K858 and the f_o-f_c map contoured at 3σ, showing the quality of the electron density map. D) Stereoplot of the magnification of the inhibitor-binding pocket. Residues, which are part of the pocket (green) and (R)-K858 (magenta), are shown as ball-and-stick models. Water molecules are shown as red cross and hydrogen bond interactions between the inhibitor and residues of Eg5 are indicated as dotted lines. Leu214, which has been shown to be crucial for conferring resistance to K858 when mutated to alanine, is coloured in black.

2.3. Molecular insights into the K858 binding pocket

The magnification of the inhibitor binding pocket with bound K858 is shown in Figure 3D. K858 binds to the allosteric inhibitor-binding pocket formed by helix α2, loop L5 and helix α3. Although additional inhibitor binding pockets have previously been identified in Eg5 such as the α4/α6 pocket, an additional site in the MT binding region and a fourth site in or close to the nucleotide binding pocket, K858 binds to the well-established allosteric pocket, which accommodates several other Eg5 inhibitor scaffolds. Although we used the racemic mixture of K858 for crystallisation of the complex we exclusively observed electron density for the (R)-enantiomer in the loop L5 pocket, indicating enantio-selectivity for K858 (Figure 3D). Enantio-selectivity has also been observed for ARRY-520 and Litronesib with the S and the R-enantiomers being the active compounds, respectively, although no structural data are available for these two thiadiazole containing clinical inhibitors yet.

Although (R)-K858 is a relatively non-sophisticated Eg5 inhibitor, compared to (S)-ARRY-520 (inhibition of the MT-stimulated Eg5 ATPase activity: IC_{50} = 6 nM, [30]) and (R)-Litronesib (inhibition of the MT-stimulated Eg5 ATPase activity: IC_{50} = 26 nM [31]), it nevertheless displays a complex network of interactions with residues in the inhibitor-binding pocket (Figure 3D). There are a variety of structural water molecules establishing interactions with (R)-K858, in particular the nitrogen atoms of the 1,3,4-thiadiazole moiety and the *N*-acetamido group. The 2-*N*-acetamido group is shielded from the solvent and points towards the interior of the inhibitor-binding pocket displaying hydrophobic interactions with Ile136, Leu160 and Phe239. The 4-acetyl group is on the opposite side of the thiadiazole ring pointing towards the solvent showing a hydrogen bond interaction with Tyr211 and some more distant water molecules. The asymmetric C_5 atom of the thiadiazole ring houses the 5-methyl and 5-phenyl groups and is the reason for K858's enantio-selectivity resulting in the active R-enantiomer. Whereas the 5-methyl group is oriented towards the solvent region, the 5-phenyl group is pointing towards a more hydrophobic portion of the binding pocket establishing hydrophobic interactions with the side chains of residues Arg119, Trp127 and Pro137. By switching the positions of two substituents, thus generating a virtual S-enantiomer, the phenyl group with a significantly larger hydrophobic character than the methyl would be placed towards the solvent region resulting in larger non-favourable interactions rationally explaining why the R-

enantiomer is favoured over the S-enantiomer. Indeed, we do not observe any electron density indicative for mixed binding of both enantiomers, further supported by the high resolution of our structure of 1.8 Å. Finally, the sulphur atom of the ring system interacts with the main chain carbonyl oxygen of Glu116, acting as the electron partner through a hydrogen bond interaction.

To further confirm enantioselectivity of Eg5 for the (*R*)-enantiomer, we resolved the racemic mixture of K858 into its enantiomers by HPLC on the polysaccharide-based IA chiral stationary phase and used the collected enantiomeric pure forms of K858 in comparative biological experiments. The first eluting enantiomer on the Chiralpak IA column has been named K858-1 and the more retained enantiomer K858-2. The enantiomer K858-1 displayed inhibitory activity at an IC_{50} of 580 ± 0.015 nM while K858-2 does not inhibit Eg5 at all, when measuring the inhibition of the basal Eg5 ATPase activity (Figure 2A). Similarly, when measuring the inhibition if the MT-stimulated ATPase acitvity, we obtained an IC_{50} of 493 ± 0.037 nM for K858-1 whereas K858-2 was inactive (Figure 2B). From ITC experiments a K_d of 220.0 ± 4.2 nM was recorded for K858-1, whereas K858-2 was again inactive (Figures 2C & D), a comparable result as obtained in ATPase activity experiments. Therefore from the biochemical assays, one could easily deduce that K858-1 is the active (*R*)-enantiomer, whereas K858-2 represents the inactive (*S*)-enantiomer, further displaying enantioselectivity.

K858 is essentially a “stripped-down” version of the two inhibitors, which reached clinical development, (S)-ARRY-520 and (R)-Litronesib, albeit already a very potent nanomolar inhibitor (Figure 1). None of the three inhibitors with a thiadiazole core moiety has been solved in complex with Eg5 and our Eg5-(R)-K858 structure allows a first glimpse into this important scaffold and how it inhibits Eg5 with exceptional potency. The thiadiazole moiety and the phenyl group are present in all three chemical structures. The substitution pattern is identical with substituents at the 2, 4 and 5 positions on the thiadiazole ring system. However, the three inhibitors vary in the nature of their substituents, which account for their different IC_{50} values, significantly better for the clinical candidates. Whereas K858 has an acetamido group in the 2-position the two clinical candidates possess either a 2,5-difluorophenyl group or a 2-pivalamide substituent. The 4-acetyl group in K858 can still be recognised in the same position on the two other clinical candidates, but as more

elaborated substituents such as the *N*-methoxy-*N*-methyl or the 4-pivaloyl substituent. This trend is even more pronounced in the 5th position, which displays a single methyl group in K858, whereas this small substituent is replaced by a 3-aminopropyl group in (S)-ARRY-520 and a sulfonamido containing substituent in Litronesib. In the case of (S)-ARRY-520 we predict that the 3-aminopropyl group is destined to interact with Glu166 in Eg5, similar to the other inhibitors containing the aminopropyl group such as STLC, ispinesib and its second generation analogue SB-743921. Although the primary amine is known to be prone to hERG liabilities, this has not been reported in any of the clinical trials for (S)-ARRY-520.

2.4. Structure-based, rational interpretation of binding of a range of K858 analogues to the Eg5 inhibitor-binding pocket

Recently, some of us [28] synthesised about one hundred K858 analogues and tested their anti-proliferative potential against the human prostate cancer cell line (PC3) and two melanoma cell lines (SK-MEL-5 and SK-MEL-28). We were capable of identifying ten compounds with anti-proliferative activity and compared the results to the control compound rK858. These results were challenging to fully interpret in terms of the SAR, because drug-like properties of these compounds such as solubility, lipophilicity and cell permeability may have significant effects in cell-based assays as opposed to cell membrane-free biochemical assays. We therefore embarked on determining the IC_{50} values of about 50 selected rK858 analogues all carrying modifications in the 5-position by quantifying the inhibition of the basal Eg5 ATPase activity. The results are summarised in Tables 1 to 4.

We first investigated the influence of the 5-methyl group on the Eg5 inhibitory activity (Table 1). Whereas analogue **2** with a 5-ethyl group displayed only a modest drop in activity (1.46 ± 0.3 μM), analogue **3** lacking the 5-methyl group displayed a significantly reduced IC_{50} value of 20.0 ± 7.3 μM, compared to 0.74 ± 0.04 μM for the parent compound **1**. A similar strong and systematic trend was observed for all other analogues that either contained or were lacking the 5-methyl group (cmpd pairs **1/3**, **26/27**, **28/29**, **33/34**, **35/36**, **41/42**, **44/45**) and will therefore not be discussed further. Exchanging the planar 5-phenyl group with a staggered cyclohexyl substituent (**4**)

led to a 10-fold drop in activity (7.5 ± 2.3 µM), indicating that the planar phenyl ring establishes better hydrophobic interactions in this part of the inhibitor-binding pocket.

Table 1: Inhibition of the basal Eg5 ATPase activity by a variety of rK858 analogues with alkyl substituents in the 5-position. MIA: Maximum inhibition attained.

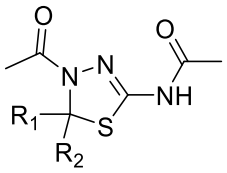

Compd No	**R_1**	**R_2**	**IC_{50} [µM] (MIA)**
1 Control rK858	Me	Ph	0.74 ± 0.04 (96)
2	Et	Ph	1.46 ± 0.3 (95)
3	H	Ph	20.0 ± 7.3 (75)
4	Me	Cyclohexyl	7.5 ± 2.3 (85)
5	Me	Me	n.i. (30)
6	Me	Et	n.i. (5)
7	Me	Pr	n.i. (30)
8	Et	Et	n.i. (35)
9	Me	*i*-Bu	n.i. (45)
10	Me	Bu	n.i. (30)
11	Et	Pr	n.i. (20)
12	Me	2-Methylprop-1-enyl	n.i. (30)
13	Me	But-3-enyl	n.i. (45)
14	Me	Pentyl	p.i. (50)
15	Et	Bu	p.i. (60)
16	Me	*n*-Hexyl	p.i. (60)

We then investigated the inhibitor effects of a range of analogues in which the 5-phenyl group was substituted with a variety of alkyl groups of varying length (cmpds **5** to **16**). Although we expected at least some inhibitory activity because placing a hydrophobic substituent into an essentially hydrophobic pocket should lead to at least some favourable interactions, to our surprise none of the tested analogues fully inhibited Eg5 activity. However, there is a clear trend between the length of the alkyl chain and the extend of inhibition with the most extended alkyl chains in this position (cmpds **15** and **16**) indicating partial inhibition of Eg5 activity of up to 60% (Table 1). From the crystal structure of Eg5-(R)-K858 complex, an interesting edge-to-face (T-shaped) aromatic stacking interaction was observed between the phenyl ring (edge) of Trp211 and phenyl group (face) of thiadiazole scaffold, which is essential for the effective binding and subsequent inhibition of Eg5 besides having good hydrophobic interactions with key residues Arg119 and Pro137. This specific edge-to-face stacking interaction was not exhibited by the analogues containing hydrophobic alkyl chains. Although being hydrophobic in nature, they can only establish weaker long distance hydrophobic interactions disfavored by a higher conformational freedom, which are, however, not sufficient for effective inhibition. In our previous published work, we had observed similar crucial edge-to-face contacts involving phenyl groups between STLC (Eg5 inhibitor) and Eg5 [32]. These data clearly identify the phenyl group as a crucial substituent of the thiadiazole scaffold for effectively inhibiting Eg5.

We then examined rK858 analogues, in which the methyl and phenyl substituents at the 5-position are combined into alicyclic substituents of increasing ring sizes and additional substituents at the cyclohexyl ring system (Table 2). Neither 5-, 6-, substituted 6-, 7- or 8-membered ring systems displayed any inhibitory activity against Eg5 thus suggesting that a certain degree of conformational freedom is requested in this position as they can be considered as cyclic analogues of derivatives **7**-**16**. In summary synthesising analogues, which combine the two substituents at the asymmetric carbon atom into non-aromatic, cyclic substituents (**17-25**) did also not lead to more potent K858 analogues.

Table 2: Inhibition of the basal Eg5 ATPase activity by a variety of rK858 analogues substituted with varying alicyclic ring systems in the 5-position. MIA: Maximum inhibition attained.

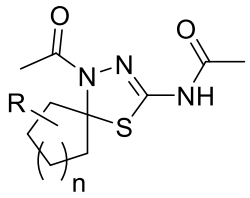

Compd No	Cycle	IC_{50} [µM] (MIA)
17	cyclopentyl	n.i. (40)
18	cyclohexyl	p.i. (60)
19	2-methylcyclohexyl	p.i. (60)
20	3-methylcyclohexyl	n.i. (40)
21	4-methylcyclohexyl	n.i. (40)
22	3,3-dimethylcyclohexyl	n.i. (10)
23	2-*tert*-butylcyclohexyl	n.i. (30)
24	cycloheptyl	n.i. (30)
25	cyclooctyl	n.i. (15)

A group of analogues incorporating various heterocyclic rings in the 5-position instead of the phenyl group resulted in a variety of active analogues (cmpds **26** to **37**, Table 3). Whereas cmpd **26**, in which the phenyl group is substituted by a furan ring system has a slightly lower IC_{50} value of 4.3 ± 0.9 µM, cmpd **28** with an unsaturated thiophen-2-yl substituent (bioisosteric replacement) displayed an IC_{50} value of 1.7 ± 0.1 µM. When the thiophene system is coordinated to the thiadiazole ring system through its 3-position, the IC_{50} is still 2.2 ± 0.3 µM. For the analogues containing an unsaturated heterocyclic ring system, the most potent analogue was cmpd **30** with a halogen substituent at the 5-position of the thiophene group. We also investigated 6-membered unsaturated pyridine substituents linked to the 5-position via the 2, 3 or 4 position of the heterocyclic pyridine ring. Whereas cmpd **33** still displays reasonable inhibitory activity against Eg5 with an IC_{50} value of 8.5 ± 0.8 µM, cmpds **32** and **35**, in

which the pyrimidine rings are linked to the 5-position of the thiadiazole scaffold via their 2- and 4-positions are significantly less active with IC_{50} values of 37.2 ± 8.8 µM and 59.9 ± 9.2 µM, respectively. Not surprisingly, cmpd **37**, containing the 1,4-diazine scaffold is a weak inhibitor of Eg5 (IC_{50} value of 46.9 ± 6.9 µM).

Table 3: Inhibition of the basal Eg5 ATPase activity by a variety of rK858 analogues with heterocyclic ring systems in the 5-position. MIA: Maximum inhibition attained.

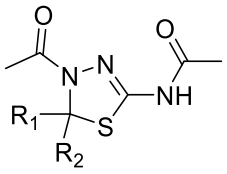

Compd No	R_1	R_2	IC_{50} [µM] (MIA)
26	Me	Furan-2-yl	4.3 ± 0.9 (95)
27	H	Furan-2-yl	n.i. (20)
28	Me	Thiophen-2-yl	1.7 ± 0.1 (95)
29	H	Thiophen-2-yl	n.i. (30)
30	Me	5-Chloro-thiophen-2-yl	0.95 ± 0.15 (95)
31	Me	Thiophen-3-yl	2.2 ± 0.3 (90)
32	Me	Pyridin-2-yl	37.2 ± 8.8 (65)
33	Me	Pyridin-3-yl	8.5 ± 0.8 (90)
34	H	Pyridin-3-yl	n.i. (30)
35	Me	Pyridin-4-yl	59.9 ± 9.2 (60)
36	H	Pyridin-4-yl	n.i (5)
37	Me	Pyrazin-2-yl	46.9 ± 6.9 (70)

Table 4 contains K858 analogues with *ortho*-, *meta*- and *para*-substitutions at the structural phenyl ring system (**38**-**42**) as well as fused ring substituents (**43**-**47**).

Compounds **41** and **42** are characterised by the same 2,5-difluoroaryl substituent present in (R)-Litronesib; the former was endowed with an inhibitory potency comparable to rK858. Cmpd **44** containing a 1-naphthyl group in the 5-position still shows good activity (IC_{50} = 1.9 µM), proving that this part of the inhibitor-binding pocket can accommodate larger aromatic substituents as long as these are planar and hydrophobic. Also in this case, the concurrent presence of a 5-methyl group was important for the inhibitory activity (compare **44**-**46**).

Table 4: Inhibition of the basal Eg5 ATPase activity by a variety of rK858 analogues with substitutions in the phenyl ring, fused aromatic and heterocyclic systems in the

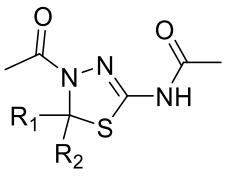

5-position. MIA: Maximum inhibition attained.

Compd No	R_1	R_2	IC_{50} [µM] (MIA)
38	Me	4-Nitrophenyl	n.i. (25)
39	Me	4-Acetylphenyl	n.i. (20)
40	Me	4-Acetyloxyphenyl	5.1 ± 0.2 (95)
41	Me	2,5-Difluorophenyl	0.84 ± 0.3 (97)
42	H	2,5-Difluorophenyl	41.1 ± 8.1 (60)
43	H	Benzo[*d*][1,3]dioxol-5-yl	n.i. (10)
44	Me	1-Naphthyl	1.9 ± 0.1 (95)
45	H	1-Naphthyl	53.9 ± 7.1 (60)
46	Me	2-Naphthyl	15.6 ± 2.6 (80)
47	Me	2-Oxo-2*H*-chromen-3-yl	n.i. (20)

Table 5 lists selected rK858 analogues with a notable inhibitory activity against Eg5 and a range of their calculated drug-like properties. Interestingly, all analogues

display favourable lipophilicity (clogP < 3.5), PSA values (<75) and good calculated solubility with the exception of cmpd **44** (calc. LogS = -4.486), which contains the much more lipophilic 1-naphthyl substituent. Remarkably, the phenyl group in rK858 is the most crucial structural requirement, responsible for imparting optimal steric and electronic properties for all analogues tested. While rK858 remains the most active Eg5 inhibitor tested in this study, compounds **28**, **30**, **31** and **41**, display inhibitory activity and ligand efficiency values close to rK858.

It is interesting to note that all three thiadiazole-based Eg5 inhibitors (Figure 1) retain the 5-phenyl group as a substituent and we can safely assume that the clinically relevant compounds such as (S)-ARRY-520 and (R)-Litronesib have certainly gone through extensive chemical optimisation of this substituent (Figure 1 & 3D), although a SAR study has not been made available for any of these clinically important drugs. This phenyl group seems to fit snuggly into this pocket and represent an ideal substituent with optimal binding features in this predominantly hydrophobic part of the pocket (Figure 4C). To gain more insights about potential structural relationships we compared all available Eg5 inhibitor scaffolds for which structural information is available in the PDB with the binding mode of K858. Interestingly, two types of scaffolds, dihydropyrrole and dihydropyrazole containing Eg5 inhibitors, which are structurally related to the thiadiazole scaffold (Figure 1, lower panel) can be fully

Table 5: Summary of inhibitory activity of rK858 and analogues against Eg5 (IC_{50} values < 4.3 µM) and some calculated drug-like properties such as ligand efficiency, clogP, solubility LogS, and polar surface area (PSA). MIA: Maximum inhibition attained.

Compd No	Analogue Structure	IC_{50} [µM] (MIA)	LE	clogP	Solubility (calc. LogS)	PSA
1 Control	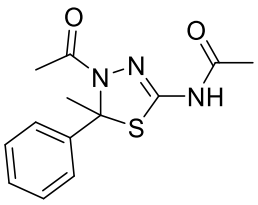	0.74 ± 0.04 (96)	0.324	2.324	-3.108	61.77

2	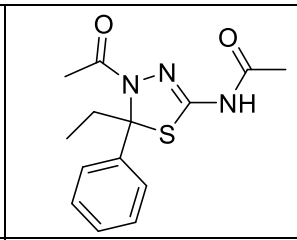	1.46 ± 0.3 (95)	0.292	2.853	-3.376	61.77
26	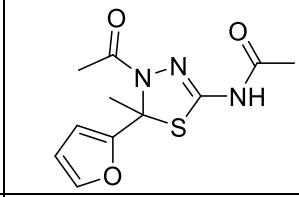	4.3 ± 0.9 (95)	0.298	1.5	-2.085	74.91
28	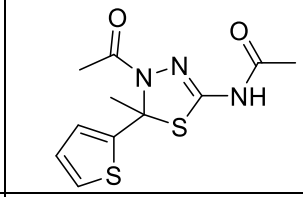	1.7 ± 0.1 (95)	0.321	1.97	-2.553	61.77
30	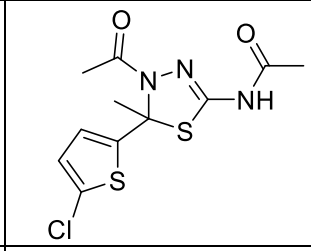	0.95 ± 0.15 (95)	0.317	2.683	-2.972	61.77
31	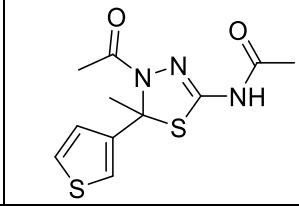	2.2 ± 0.3 (90)	0.314	1.97	-2.768	61.77
41	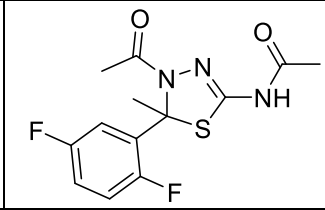	0.84 ± 0.3 (97)	0.289	0.308	-3.643	61.77
51	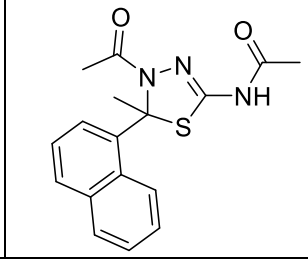	1.9 ± 0.1 (95)	0.249	3.498	-4.486	61.77

overlaid with (R)-K858, displaying the same binding mode (Figures 4A and B): all scaffolds show the same substitution pattern with the thiadiazole, dihydropyrrole and dihydropyrazole ring systems at the same position, as in the case of the unsubstituted phenyl group. The 2,5-difluorophenyl substituent can be found in two

clinical candidate molecules such as MK-0731 and (S)-ARRY-520 (Figure 1). The combination of medicinal chemistry efforts from Merck by combining the dihydropyrrole and dihydropyrazole scaffolds resulted in the MK-0731 [33]. Although the chemical and the structural resemblance as well as their mode of action on Eg5 of both candidates is fully obvious, it clearly demonstrates how important small differences in promising candidate compounds can be: whereas MK-0731 is mostly insoluble and did not proceed past phase I clinical trials, its more successful “brother” entered phase III clinical trails against multiple myeloma.

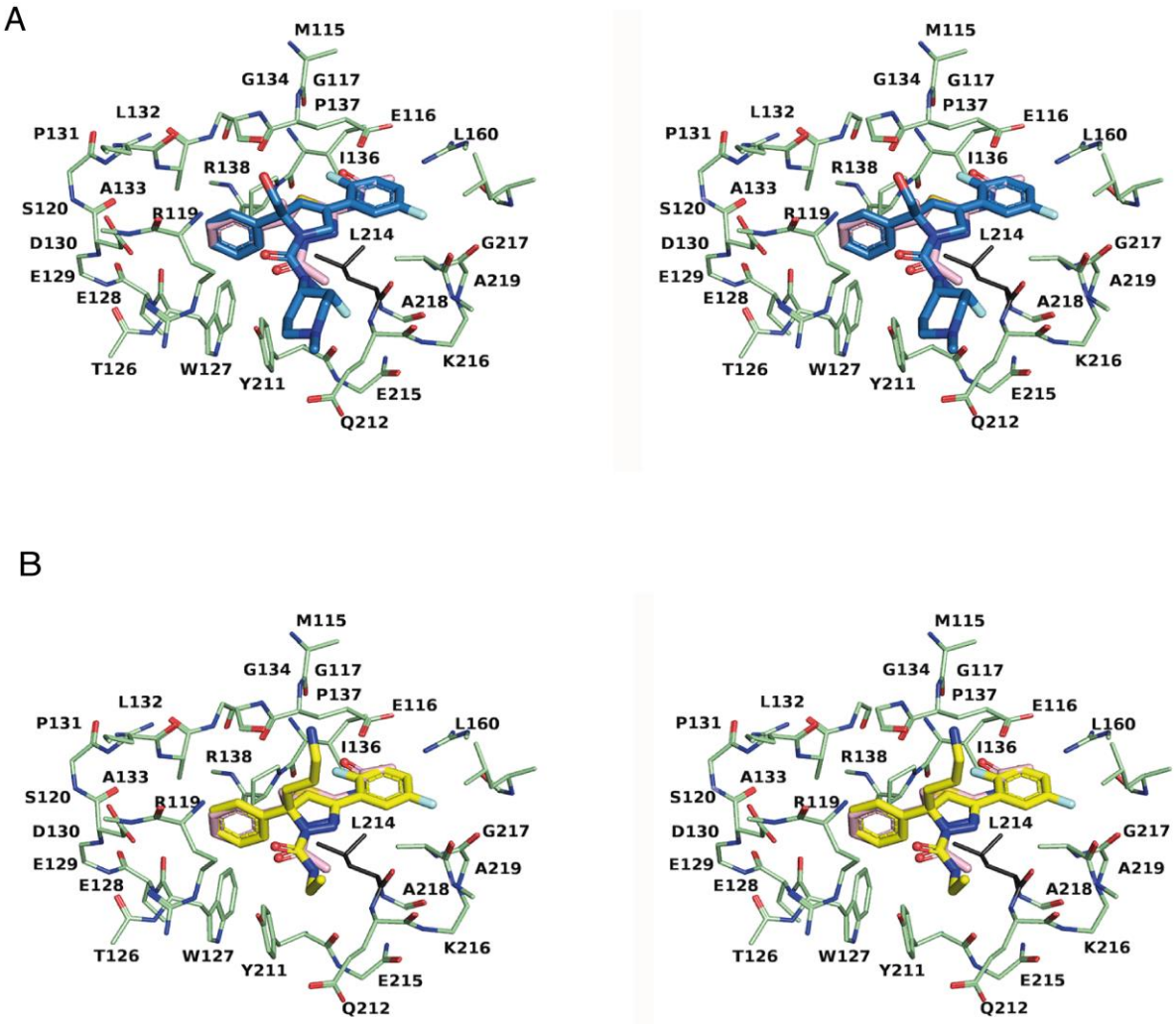

Figure 4: Comparision of the interactions of different chemical scaffolds with key residues of the allosteric Eg5 inhibitor-binding pocket. A) Stereoplot of the magnification of the inhibitor-binding pocket showing the overlay of (R)-K858 (thiadiazole core, magenta) and MK-0731 (dihydropyrrole core, blue, PDB ID: 3CJO, [33]). B) Stereoplot of the overlay between (R)-K858 (magenta) and a dihydropyrazole containing scaffold (yellow, PDB ID: 2G1Q, [34]). All three core structures possess the same substitution pattern and the core as well as the phenyl groups are located in the same part of the inhibitor - binding pocket.

3. Conclusions

In this study we determined the crystal structure of an Eg5-inhibitor complex containing the 1,3,4-thiadiazole core scaffold, which is present in clinically relevant Eg5 targeting inhibitors such as (S)-ARRY-520 and (R)-Litronesib. We were also able to determine the IC_{50} values of 46 K858 analogues by measuring the inhibition of the basal Eg5 ATPase activity and based on the structural insights gained from the complex we could use this structure for rationalising our SAR study. This will serve as a basis for future structure-based drug design of this very important chemical scaffold.

4. Materials and methods

4.1. Chemistry

All chemicals and reagents (AR grade) were purchased from Sigma–Aldrich and Merck Millipore, South Africa. Solvents except laboratory reagent grade were dried and purified as per the reported literature methods when necessary. The progress of reactions and purity of compounds were monitored by thin-layer chromatography (TLC) on pre-coated aluminum silica gel plates procured from E. Merck and Co. (Darmstadt, Germany) using methanol (10%) in chloroform as mobile phase and iodine vapor as a visualising agent. The ^{1}H NMR and ^{13}C NMR were recorded on a Bruker AVANCE 400 and 100 MHz (Bruker, Rheinstetten/Karlsruhe, Germany) using DMSO-d_6 or $CDCl_3$. Chemical shifts are reported in δ ppm units with respect to TMS as an internal standard.

4.1 Synthesis of racemic K858

Racemic K858 was synthesised as previously described [27, 28].

*(E)-2-(1-phenylethylidene)hydrazine-1-carbothioamide (**c**)*

To a solution of acetophenone **a** (33.3 mmol, 4 g) and thiosemicarbazide (**b**) (34.6 mmol, 3.15 g) in 90 ml of methanol, 0.3 ml of concentrated hydrochloric acid was slowly added dropwise and stirred for 15 h. After completion of the reaction (as monitored by TLC), 30 ml of water was added to the mixture to obtain product **c**. The obtained solids were filtered and washed with diisopropyl ether to yield white crystals

of **b** in pure form (4.7 g, 81% yield). ^{1}H NMR (400 MHz, DMSO-d_6) δ: 2.30 (s, 3H, CH_3), 7.37 – 7.39 (m, 3H, ArH), 7.91 – 7.93 (m, 2H, ArH, 1H, NH_2), 8.27 (s, 1H, NH_2), 10.2 (s, 1H, NH) ppm; ^{13}C NMR (100 MHz, DMSO-d_6) δ: 14.0 ($\underline{C}H_3$), 126.6, 128.2, 129.1, 137.6, 147.8, 178.9 ppm.

*N-(4-acetyl-5-methyl-5-phenyl-4,5-dihydro-1,3,4-thiadiazol-2-yl)acetamide (**1**) or K858*

Compound **c** (0.889 mmol; 0.3 g) in acetic anhydride (11 mmol; 1 ml) was refluxed until a homogenous mixture appeared. Then, the solution was cooled to room temperature to obtain compound **1**. Diethyl ether (120 ml) was added to remove non-polar impurities to yield white crystals which were dried under vacuum (0.413g, 86 %). ^{1}H NMR (400 MHz, DMSO-d_6) δ: 2.01 (s, 3H, CH_3), 2.19 (s, 3H, CH_3), 2.28 (s, 3H, CH_3), 7.24 – 7.25 (s, 1H, ArH), 7.25 – 7.35 (m, 4H, ArH), 11.63 (s, 1H, NH) ppm; ^{13}C NMR (100 MHz, DMSO-d_6) δ: 22.4, 23.7, 26.6 (3$\underline{C}H_3$), 78.6, 124.4, 127.3, 128.4, 142.2, 143.8, 167.7 and 169.3 (2$\underline{C}$=O) ppm.

The syntheses and characterisation of the other 46 rK858 analogues (**2**-**46**) have recently been described in detail [26].

4.2 Enantioselective HPLC.

Enantioselective HPLC analyses were performed by using stainless-steel Chiralpak IA (250 mm × 4.6 mm i.d. and 250 mm × 10 mm i.d.) (Daicel, Chemical Industries, Tokyo, Japan) columns. HPLC-grade solvents were used as supplied by Aldrich (Milan, Italy). The HPLC apparatus consisted of a PerkinElmer (Norwalk, CT, USA) 200 LC pump equipped with a 542 Rheodyne (Cotati, CA, USA) injector, a 1000 µL sample loop, a HPLC Perkin-Elmer oven and a Perkin-Elmer 290 detector. The signal was acquired and processed by Clarity software (DataApex, Prague, The Czech Republic).

4.3 Subcloning, expression and purification of human Eg5

The human $Eg5_{1\text{-}368}$ motor domain was expressed and purified as previously described [32].

4.4 Steady-state ATPase activity assays

Steady-state basal and MT-stimulated Eg5 ATPase activities were measured using the pyruvate kinase (PK)-lactate dehydrogenase (LDH) coupled assay as described [35]. The quantities of Eg5 used in the basal and MT-stimulated conditions were 150 nM and 10 nM, respectively. The Mg^{2+}ATP concentration was fixed at 1 mM and the MT-stimulated ATPase activity was carried out in the presence of 1 µM MTs. For the inhibition of the basal Eg5 ATPase activity, assays were carried out in the presence of 150 mM KCl, whereas in the presence of MTs, no salt was added to the buffer conditions. ATPase measurements were performed at 25°C using a 96-well Sunrise photometer (Tecan, Mannesdorf, Switzerland). The IC_{50} values were calculated using Kaleidagraph 4.0 (Synergy Software). MTs were polymerised from lyophilised tubulin (Tebu-Bio catalogue No. 027T240-B) as described in [36].

4.5 *Isothermal titration calorimetry (ITC)*

Interactions between Eg5 and K858 were studied by ITC using a MicroCal PEAQ-ITC (Malvern) as previously described, but with some modifications [37, 38]. Prior to ITC analysis, Eg5 was dialysed in dialysis buffer (20 mM PIPES pH 6.9, 250 mM NaCl, 2 mM β-mercaptoethanol, 0.5 mM ADP) overnight at 4°C. For the ITC analysis, Eg5 was used at 10 µM and rK858, K858-1 and K858-2 at 100 µM. To compensate for additional DMSO in the inhibitor solution, 1% DMSO was added to Eg5 before the experiment. rK858 and its enantiomers were titrated into the Eg5 solution in 30 injections with spacing of 120 sec between each injection and a constant stirring speed of 750 rpm. To calculate heats of dilution, rK858 and its enantiomers were injected into buffer with 1% DMSO that was subtracted prior to data analysis using the MicroCal PEAQ-ITC Analysis Software (Malvern). All ITC experiments were performed at 25°C. The measured thermodynamic parameters n (stoichiometry), K_a (association constant) and ΔH (enthalpy change) were acquired through fitting of the experimental data using the single-site binding model. The binding free energy (ΔG) and entropy change (ΔS) were then calculated from the fitted values. The ITC analysis was performed in duplicate and the averaged values are presented.

4.6 Crystallisation of the Eg5-rK858 complex

Purified Eg5 (10 mg/mL) was incubated with 1 mM rK858 and 1 mM Mg^{2+}ATP overnight at 4°C. Following incubation, the sample was centrifuged at 13,000 rpm for 10 min at 4°C to remove any protein aggregate or undissolved inhibitor. The complex was then used to set up crystallisation trials.

Crystal obtained in space group $C222_1$: Needle-like crystals of the complex appeared overnight at 18°C in hanging drops consisting of 1 µl Eg5-rK858 complex and 1 µl reservoir solution (0.1 M HEPES pH 8.0, 12.5% PEG3350, and 0.1 M $MgCl_2$). The crystals initially obtained did not diffract to a minimum threshold resolution required to study protein-inhibitor interactions. Therefore, we employed crystal dehydration techniques. Crystals were transferred to different drops to allow further vapour diffusion with increasing amounts of PEG3350 with increments of 0.5% to 10% compared to the amount originally present in the reservoir solution. The time for dehydration varied between three days to a week. Eventually, plate-like crystals appeared and these crystals diffracted to a significantly higher resolution compared to the original needle-like crystals.

Crystals obtained in space group $P6_522$: Rhombohedral shaped crystals appeared after a fortnight in a mixture of 1 µl of the Eg5-rK858 complex and 1 µl of the reservoir solution containing 0.1 M MES, pH 5.5, 24.5% PEG3350, 0.3 M $(NH_4)_2SO_4$ and 0.1 M Trimethylamine at 4°C.

Crystals from both conditions were cryoprotected in a solution containing 1.2 fold of the crystallisation solution present in the reservoir supplemented with ~15% glycerol and flash-frozen in liquid nitrogen for subsequent data collection.

4.7 Data collection, structure determination, refinement and model quality

Diffraction data for the two distinct crystal forms were collected at the European Synchrotron Radiation Facility (ESRF), beamline ID30A-1. Data were processed using either XDS [39] or iMosflm [40] and scaled to resolutions as mentioned in Table 6 [41]. The structures of the Eg5-rK858 complex were solved in two space groups by molecular replacement (PHASER MR in CCP4 suite) using a previously published Eg5 structure (PDB ID: 1X88,[42]) as a search model. All structures were initially

refined with REFMAC5 [43]. Electron density and difference density maps, all σA-weighted, were inspected, and the models were improved using Coot [44]. Further refinement of the structures was performed using PHENIX [45]. The calculation of R_{free} used 5% of data. Crystallographic and refinement statistics are given in Table 6.

Both space groups contain one Eg5-rK858 complex per AU. The complexes cover residues Lys17 to Glu364 and Asn18 to Glu367 in space groups $C222_1$ and $P6_522$, respectively. In the former space group, loops containing residues 56-60, 176-179, 249-243 and 272-286 are missing in the structure, whereas in the latter space group the regions 34-35 and 272-287 are absent.

Table 6: Data collection, structure determination and refinement statistics for the ternary ADP-Eg5–(R)-K858 complex.[a, b]

Statistics	**Eg5-(R)-K858 complex in space group $C222_1$**	**Eg5-(R)-K858 complex in space group $P6_522$**
PDB ID	6G6Y	6G6Z
Beamline	ID30A-1	ID30A-1
Molecules per asymmetric unit	1	1
Resolution range [Å]	50 - 1.8	50 - 2.8
Unit cell parameters [Å, °]	a = 62.5, b = 108.4, c = 111.4, α = β = γ = 90	a = b = 100.3, c = 185.4, α = β = 90, γ = 120
Completeness [%]	96.0 (93.5)	99.3 (96.5)
R_{merge}	2.9 (51.6)	2.1 (41.8)
Multiplicity	1.9 (1.8)	2.0 (3.3)

Mean I/σ(I)	13.9 (2.1)	22.8 (1.8)
CC1/2	99.9 (77.4)	99.9 (79.9)
Total reflections	64132 (5878)	28050 (2454)
Unique reflections	33988 (3262)	14182 (1326)
Wilson B-factor (Å^2)	26.5	75.7
Refinement statistics		
R_{work} / R_{free} [%]	21.2 / 25.6	23.9 / 26.1
Average B-factor (Å^2):		
- Overall	37.2	77.3
- Eg5 motor domain	37.1	77.6
- Solvent	41.2	70.2
- Mg^{2+}ADP	25.8	70.9
- (R)-K858	25.7	76.3
No. of Mg^2ADP / Inhibitor / water	1 / 1 / 229	1 / 1 / 41
r.m.s.d. bond lengths [Å]	0.012	0.013
r.m.s.d. bond angles [°]	1.48	1.56
Ramachandran plot statistics (%):		
- Favoured	98.4	96.6
- Allowed	1.6	2.2
- Outliers	0.0	1.2

[a]The racemic mixture of K858 was used for crystallisation. [b]Values in parentheses pertain to the highest-resolution shell.

Author contributions

The manuscript was written through contributions of all authors. All authors have given approval to the final version of the manuscript. This publication contains part of the doctoral thesis of CLT.

Acknowledgements

We acknowledge the European Synchrotron Radiation Facility for provision of synchrotron radiation facilities and we would like to thank Matthew Bowler and Didier Nurizzo for assistance in using beamline ID30A-1 (Massif-1). Simone Carradori kindly acknowledges Prof. Ida Silvestri for the preliminary studies involving prostate and melanoma cell lines.

Funding

We are grateful to the UCL School of Pharmacy to financially support this project. BC and RK are thankful to the College of Health Sciences, University of KwaZulu-Natal (UKZN) and National Research Foundation (NRF), South Africa for funding the project (Grant No. 99546, 103728 and 112079).

Conflict of interest

The authors declare no conflict of interest.

References

[1] M.A. Jordan, L. Wilson, Microtubules as a target for anticancer drugs, Nature reviews. Cancer, 4 (2004) 253-265.

[2] G.A. Orr, P. Verdier-Pinard, H. McDaid, S.B. Horwitz, Mechanisms of Taxol resistance related to microtubules, Oncogene, 22 (2003) 7280-7295.

[3] M. Kavallaris, Microtubules and resistance to tubulin-binding agents, Nature reviews. Cancer, 10 (2010) 194-204.

[4] G. Cavaletti, P. Marmiroli, Chemotherapy-induced peripheral neurotoxicity, Nature reviews. Neurology, 6 (2010) 657-666.

[5] H. Miki, M. Setou, N. Hirokawa, Kinesin superfamily proteins (KIFs) in the mouse transcriptome, Genome research, 13 (2003) 1455-1465.

[6] A. Blangy, H.A. Lane, P. d'Herin, M. Harper, M. Kress, E.A. Nigg, Phosphorylation by p34cdc2 regulates spindle association of human Eg5, a kinesin-related motor essential for bipolar spindle formation in vivo, Cell, 83 (1995) 1159-1169.

[7] A.S. Kashina, R.J. Baskin, D.G. Cole, K.P. Wedaman, W.M. Saxton, J.M. Scholey, A bipolar kinesin, Nature, 379 (1996) 270-272.

[8] R.K. Phillips, L.G. Peter, S.P. Gilbert, I. Rayment, Family-specific Kinesin Structures Reveal Neck-linker Length Based on Initiation of the Coiled-coil, J Biol Chem, 291 (2016) 20372-20386.

[9] L.C. Kapitein, E.J. Peterman, B.H. Kwok, J.H. Kim, T.M. Kapoor, C.F. Schmidt, The bipolar mitotic kinesin Eg5 moves on both microtubules that it crosslinks, Nature, 435 (2005) 114-118.

[10] T.U. Mayer, T.M. Kapoor, S.J. Haggarty, R.W. King, S.L. Schreiber, T.J. Mitchison, Small molecule inhibitor of mitotic spindle bipolarity identified in a phenotype-based screen, Science (New York, N.Y.), 286 (1999) 971-974.

[11] J.R. Infante, R. Kurzrock, J. Spratlin, H.A. Burris, S.G. Eckhardt, J. Li, K. Wu, J.M. Skolnik, L. Hylander-Gans, A. Osmukhina, D. Huszar, R.S. Herbst, A Phase I study to assess the safety, tolerability, and pharmacokinetics of AZD4877, an intravenous Eg5 inhibitor in patients with advanced solid tumors, Cancer chemotherapy and pharmacology, 69 (2012) 165-172.

[12] H.A. Burris, 3rd, S.F. Jones, D.D. Williams, S.J. Kathman, J.P. Hodge, L. Pandite, P.T. Ho, S.A. Boerner, P. Lorusso, A phase I study of ispinesib, a kinesin spindle protein inhibitor, administered weekly for three consecutive weeks of a 28-day cycle in patients with solid tumors, Investigational new drugs, 29 (2011) 467-472.

[13] K. Holen, R. DiPaola, G. Liu, A.R. Tan, G. Wilding, K. Hsu, N. Agrawal, C. Chen, L. Xue, E. Rosenberg, M. Stein, A phase I trial of MK-0731, a kinesin spindle protein (KSP) inhibitor, in patients with solid tumors, Investigational new drugs, 30 (2012) 1088-1095.

[14] K.D. Holen, C.P. Belani, G. Wilding, S. Ramalingam, J.L. Volkman, R.K. Ramanathan, L.S. Vasist, C.J. Bowen, J.P. Hodge, M.M. Dar, P.T. Ho, A first in human study of SB-743921, a kinesin spindle protein inhibitor, to determine pharmacokinetics, biologic effects and establish a recommended phase II dose, Cancer chemotherapy and pharmacology, 67 (2011) 447-454.

[15] O. Rath, F. Kozielski, Kinesins and cancer, Nature Reviews Cancer, 12 (2012) 527.

[16] B. Owens, Kinesin inhibitor marches toward first-in-class pivotal trial, Nature medicine, 19 (2013) 1550.

[17] J.E.R. Shelley Allen, Qian Zhao, Jeremy Hans, Joe Lyssikatos, Tom Aicher, Chris Corrette, Ellen R. Laird, Kirk DeLisle, Walter Voegtli, Christine Lemieux, Stefan Gross, Walter E. DeWolf Jr., Rich Woessner, Patrice Lee, Gregory Poch, Jennifer Otten, Michelle Livingston, Gary Hingorani, Andrew Allen , Eli Wallace. , The discovery and optimization of kinesin spindle protein (KSP) inhibitors: path to ARRY-520. , in: Cambridge Healthtech Institute conference, 2012.

[18] X. Ye, W.L. Tam, T. Shibue, Y. Kaygusuz, F. Reinhardt, E. Ng Eaton, R.A. Weinberg, Distinct EMT programs control normal mammary stem cells and tumour-initiating cells, Nature, 525 (2015) 256-260.

[19] H. Wakui, N. Yamamoto, S. Kitazono, H. Mizugaki, S. Nakamichi, Y. Fujiwara, H. Nokihara, Y. Yamada, K. Suzuki, H. Kanda, S. Akinaga, T. Tamura, A phase 1 and dose-finding study of LY2523355 (litronesib), an Eg5 inhibitor, in Japanese patients with advanced solid tumors, Cancer chemotherapy and pharmacology, 74 (2014) 15-23.

[20] J.R. Infante, A. Patnaik, C.F. Verschraegen, A.J. Olszanski, M. Shaheen, H.A. Burris, A.W. Tolcher, K.P. Papadopoulos, M. Beeram, S.M. Hynes, J. Leohr, A.B. Lin, L.Q. Li, A. McGlothlin, D.L. Farrington, E.H. Westin, R.B. Cohen, Two Phase 1 dose-escalation studies exploring multiple regimens of litronesib (LY2523355), an Eg5 inhibitor, in patients with advanced cancer, Cancer chemotherapy and pharmacology, 79 (2017) 315-326.

[21] S.W. Baertschi, P.J. Jansen, R.M. Montgomery, W.K. Smith, J.R. Draper, D.P. Myers, P.G. Houghton, V.S. Sharp, A.L. Guisbert, H. Zhuang, M.A. Watkins, G.A. Stephenson, T.M. Harris, Investigation of the mechanism of racemization of litronesib in aqueous solution: unexpected base-catalyzed inversion of a fully substituted carbon chiral center, J Pharm Sci, 103 (2014) 2797-2808.

[22] R. Williams, Discontinued in 2013: oncology drugs, Expert Opin Investig Drugs, 24 (2015) 95-110.

[23] R. Nakai, S. Iida, T. Takahashi, T. Tsujita, S. Okamoto, C. Takada, K. Akasaka, S. Ichikawa, H. Ishida, H. Kusaka, S. Akinaga, C. Murakata, S. Honda, M. Nitta, H. Saya, Y. Yamashita, K858, a novel inhibitor of mitotic kinesin Eg5 and antitumor agent, induces cell death in cancer cells, Cancer research, 69 (2009) 3901-3909.

[24] L. Taglieri, G. Rubinacci, A. Giuffrida, S. Carradori, S. Scarpa, The kinesin Eg5 inhibitor K858 induces apoptosis and reverses the malignant invasive phenotype in human glioblastoma cells, Investigational new drugs, 36 (2018) 28-35.

[25] F. De Iuliis, L. Taglieri, G. Salerno, A. Giuffrida, B. Milana, S. Giantulli, S. Carradori, I. Silvestri, S. Scarpa, The kinesin Eg5 inhibitor K858 induces apoptosis but also survivin-related chemoresistance in breast cancer cells, Investigational new drugs, 34 (2016) 399-406.

[26] C. Murakata, K. Kato, Y. Ohta, R. Nakai, Y. Yamashita, T. Takahashi, Y. Ino, THIADIAZOLINE DERIVATIVE in, Japan, 26.06.2003.

[27] J. Yamamoto, N. Amishiro, K. Kato, Y. Ohta, Y. Ino, M. Araki, T. Tsujita, S. Okamoto, T. Takahashi, H. Kusaka, S. Akinaga, Y. Yamashita, R. Nakai, C. Murakata, Synthetic studies on mitotic kinesin Eg5 inhibitors: synthesis and structure-activity relationships of novel 2,4,5-substituted-1,3,4-thiadiazoline derivatives, Bioorg Med Chem Lett, 24 (2014) 3961-3963.

[28] C. De Monte, S. Carradori, D. Secci, M. D'Ascenzio, P. Guglielmi, A. Mollica, S. Morrone, S. Scarpa, A.M. Agliano, S. Giantulli, I. Silvestri, Synthesis and pharmacological screening of a large library of 1,3,4-thiadiazolines as innovative therapeutic tools for the treatment of prostate cancer and melanoma, Eur J Med Chem, 105 (2015) 245-262.

[29] R.L. Indorato, S. DeBonis, F. Kozielski, I. Garcia-Saez, D.A. Skoufias, STLC-resistant cell lines as tools to classify chemically divergent Eg5 targeting agents according to their mode of action and target specificity, Biochemical pharmacology, 86 (2013) 1441-1451.

[30] B.Z. Carter, D.H. Mak, R. Woessner, S. Gross, W.D. Schober, Z. Estrov, H. Kantarjian, M. Andreeff, Inhibition of KSP by ARRY-520 induces cell cycle block and cell death via the mitochondrial pathway in AML cells, Leukemia, 23 (2009) 1755-1762.

[31] X.S. Ye, L. Fan, R.D. Van Horn, R. Nakai, Y. Ohta, S. Akinaga, C. Murakata, Y. Yamashita, T. Yin, K.M. Credille, G.P. Donoho, F.F. Merzoug, H. Li, A. Aggarwal, K. Blanchard, E.H. Westin, A Novel Eg5 Inhibitor (LY2523355) Causes Mitotic Arrest and Apoptosis in Cancer Cells and Shows Potent Antitumor Activity in Xenograft Tumor Models, Mol Cancer Ther, 14 (2015) 2463-2472.

[32] H.Y. Kaan, V. Ulaganathan, D.D. Hackney, F. Kozielski, An allosteric transition trapped in an intermediate state of a new kinesin-inhibitor complex, The Biochemical journal, 425 (2009) 55-60.

[33] C.D. Cox, P.J. Coleman, M.J. Breslin, D.B. Whitman, R.M. Garbaccio, M.E. Fraley, C.A. Buser, E.S. Walsh, K. Hamilton, M.D. Schaber, R.B. Lobell, W. Tao, J.P. Davide, R.E. Diehl, M.T. Abrams, V.J. South, H.E. Huber, M. Torrent, T. Prueksaritanont, C. Li, D.E. Slaughter, E. Mahan, C. Fernandez-Metzler, Y. Yan, L.C. Kuo, N.E. Kohl, G.D. Hartman, Kinesin spindle protein (KSP) inhibitors. 9. Discovery of (2S)-4-(2,5-difluorophenyl)-n-[(3R,4S)-3-fluoro-1-methylpiperidin-4-yl]-2-(hydrox

ymethyl)-N-methyl-2-phenyl-2,5-dihydro-1H-pyrrole-1-carboxamide (MK-0731) for the treatment of taxane-refractory cancer, J Med Chem, 51 (2008) 4239-4252.

[34] C.D. Cox, M. Torrent, M.J. Breslin, B.J. Mariano, D.B. Whitman, P.J. Coleman, C.A. Buser, E.S. Walsh, K. Hamilton, M.D. Schaber, R.B. Lobell, W. Tao, V.J. South, N.E. Kohl, Y. Yan, L.C. Kuo, T. Prueksaritanont, D.E. Slaughter, C. Li, E. Mahan, B. Lu, G.D. Hartman, Kinesin spindle protein (KSP) inhibitors. Part 4: Structure-based design of 5-alkylamino-3,5-diaryl-4,5-dihydropyrazoles as potent, water-soluble inhibitors of the mitotic kinesin KSP, Bioorg Med Chem Lett, 16 (2006) 3175-3179.

[35] D.D. Hackney, W. Jiang, Assays for kinesin microtubule-stimulated ATPase activity, Methods in molecular biology (Clifton, N.J.), 164 (2001) 65-71.

[36] F. Kozielski, S. DeBonis, D.A. Skoufias, Screening for Inhibitors of Microtubule-Associated Motor Proteins, in: J. Zhou (Ed.) Microtubule Protocols, Humana Press, Totowa, NJ, 2007, pp. 189-207.

[37] P.R. Sheth, A. Basso, J.S. Duca, C.A. Lesburg, P. Ogas, K. Gray, L. Nale, A.F. Mannarino, A.J. Prongay, H.V. Le, Thermodynamics of nucleotide and inhibitor binding to wild-type and ispinesib-resistant forms of human kinesin spindle protein, Biochemistry, 48 (2009) 11045-11055.

[38] S.K. Talapatra, A.W. Schuttelkopf, F. Kozielski, The structure of the ternary Eg5-ADP-ispinesib complex, Acta crystallographica. Section D, Biological crystallography, 68 (2012) 1311-1319.

[39] W. Kabsch, Xds, Acta crystallographica. Section D, Biological crystallography, 66 (2010) 125-132.

[40] T.G. Battye, L. Kontogiannis, O. Johnson, H.R. Powell, A.G. Leslie, iMOSFLM: a new graphical interface for diffraction-image processing with MOSFLM, Acta crystallographica. Section D, Biological crystallography, 67 (2011) 271-281.

[41] M.D. Winn, C.C. Ballard, K.D. Cowtan, E.J. Dodson, P. Emsley, P.R. Evans, R.M. Keegan, E.B. Krissinel, A.G. Leslie, A. McCoy, S.J. McNicholas, G.N. Murshudov, N.S. Pannu, E.A. Potterton, H.R. Powell, R.J. Read, A. Vagin, K.S. Wilson, Overview of the CCP4 suite and current developments, Acta crystallographica. Section D, Biological crystallography, 67 (2011) 235-242.

[42] Z. Maliga, T.J. Mitchison, Small-molecule and mutational analysis of allosteric Eg5 inhibition by monastrol, BMC Chem Biol, 6 (2006) 2.

[43] G.N. Murshudov, A.A. Vagin, E.J. Dodson, Refinement of macromolecular structures by the maximum-likelihood method, Acta crystallographica. Section D, Biological crystallography, 53 (1997) 240-255.

[44] P. Emsley, K. Cowtan, Coot: model-building tools for molecular graphics, Acta crystallographica. Section D, Biological crystallography, 60 (2004) 2126-2132.

[45] P.D. Adams, P.V. Afonine, G. Bunkoczi, V.B. Chen, I.W. Davis, N. Echols, J.J. Headd, L.W. Hung, G.J. Kapral, R.W. Grosse-Kunstleve, A.J. McCoy, N.W. Moriarty, R. Oeffner, R.J. Read, D.C. Richardson, J.S. Richardson, T.C. Terwilliger, P.H.

Zwart, PHENIX: a comprehensive Python-based system for macromolecular structure solution, Acta crystallographica. Section D, Biological crystallography, 66 (2010) 213-221.